Mechanics of Materials 140 (2020) 103217

Contents lists available at ScienceDirect

Mechanics of Materials

journal homepage: www.elsevier.com/locate/mechmat

Research paper

Damage mechanism and dynamic constitutive model of frozen soil under uniaxial impact loading

Fulai Zhang[a], Zhiwu Zhu[a,b,*], Tiantian Fu[a], Jinxuan Jia[a]

[a] Applied Mechanics and Structure Safety Key Laboratory of Sichuan Province, School of Mechanics and Engineering, Southwest Jiaotong University, Chengdu, Sichuan, China

[b] State Key laboratory of Traction Power, Southwest Jiaotong University, Chengdu, Sichuan, China

ARTICLE INFO

Keywords:
Frozen soil
SHPB
Saturated crack
Damage
ZWT model

ABSTRACT

The dynamic mechanical properties of frozen soil at different temperatures and high strain rates were tested using a split Hopkinson pressure bar (SHPB), and the variation of the wave impedance of the frozen soil was analyzed. Viscoelastic theory confirmed that an increase in the wave impedance in frozen soil over short times is the result of unfrozen water relaxation. Unfrozen water is an important factor that increases the peak stress of frozen soil under impact loading. Based on the compression failure mechanism of frozen soil, the internal microcracks were classified as random or vertical microcracks. The mesoscopic parameter (microcrack density) and the macroscopic physical quantity (wave velocity) were connected by the effective medium theory, and the longitudinal wave velocity was selected as the damage variable. The effects of the low-frequency parameters in the ZWT (Zhu–Wang–Tang) model (Wang, 2003) when applied to frozen soil were evaluated. Under impact-loading conditions, with the initiation and expansion of the internal microcracks in the frozen soil, the Maxwell element represented by the low-frequency parameters lost its function rather than degenerating into a simple spring, and thus, it continued to contribute to the macroscopic mechanical properties of the frozen soil. Finally, damage was introduced into the improved ZWT model to establish a dynamic constitutive model of the frozen soil. The predicted and experimental results agreed well, which verified the applicability of the model.

1. Introduction

Frozen soil is a complex multiphase medium due to partial water freezing when the temperature drops to 0 ˚C or below. It is composed mainly of soil particles, ice, unfrozen water, and air. The permafrost region of the world accounts for about 24% of the total land area (French, 2017). Owing to the increase in human activities, a large number of construction and maintenance projects in cold regions are facing problems associated with frozen soil. The existence of ice changes the interlinking characteristics of each phase in frozen soil, which causes the mechanical properties of frozen soil to differ significantly from those of thawed soil. The mechanical behavior of frozen soil, as a complex multiphase medium, is affected by the coupling between the permeability field, stress field, temperature field, and ice–water phase transition (Ma and Wang, 2012). Damage theory is a powerful tool for modeling this complex multiphase medium deformation problem (Lemaitre, 1990). Miao et al. (1995) studied the microstructural damage of frozen loess by scanning electron microscopy (SEM), and a constitutive model of the viscoplastic damage was presented using the ice content as the damage variable. He et al. (1999) presented a constitutive model of the viscoelastic–plastic damage of frozen soil based on continuum mechanics and thermodynamic laws. Zhu et al. (2010) presented a constitutive model of the elastic damage of frozen soil based on the law of mixtures and stochastic damage theory.

As a carrier in cold region environments, frozen soil is often subjected to various forms of impact loading in practical engineering. Under impact loading, the duration of the stress wave is usually 100–200 μs, and thus, characterizing the mesoscopic damage parameters of the materials quantitatively is difficult. Xie et al. (2016) assumed that the frozen soil was composed of a soil matrix and ice particles and that the damage behavior of the frozen soil was due to the debonding of the interface between the soil matrix and ice particles. They presented a constitutive model for the dynamic damage of frozen soil. Ma et al. (2017) believed that the damage followed a Weibull distribution and presented a constitutive model of the dynamic damage

* Corresponding author at: Applied Mechanics and Structure Safety Key Laboratory of Sichuan Province, School of Mechanics and Engineering, Southwest Jiaotong University, Chengdu Sichuan 610031, China.
E-mail address: zzw4455@163.com (Z. Zhu).

https://doi.org/10.1016/j.mechmat.2019.103217
Received 30 July 2019; Received in revised form 19 September 2019; Accepted 18 October 2019
Available online 25 October 2019

based on the ZWT (Zhu–Wang–Tang) model. Cao et al. (2018) assumed that the damage of frozen soil was a viscoplastic deformation process related to the strain rate. By introducing strain rate strengthening and temperature softening effects into the constitutive model, a dynamic damage model was proposed that could describe the strain rate and temperature effects. In addition, Zhang et al. (2013) and Ma et al. (2019a, 2019b) explored the dynamic mechanical properties of frozen soil under a confining pressure and coupled static–dynamic loading, respectively, using split Hopkinson pressure bar (SHPB) devices. In many existing dynamic constitutive models, the frozen soil is considered to be composed primarily of soil and ice. However, unfrozen water is always present in the negative temperature range (Fortin et al., 2011; Zhang et al., 2018). Under quasi-static loading, unfrozen water does not significantly affect the evolution process of cracks. However, under impact loading, the evolution process of microcracks containing fluid is influenced by the Stefan effect (Rossi and Toutlemonde, 1996). Saturated cracks can be considered to be in an undrained state under a high strain rate (Li, 2014), which significantly influences the strengths of the materials (Zhou et al., 2019). Therefore, the effect of unfrozen water on the dynamic mechanical properties of frozen soil is worthy of study and should be included in the constitutive model.

In this study, the dynamic mechanical properties of frozen soil were tested using a SHPB at different temperatures (−10 to −20 °C) and high strain rates (400–950 s^{-1}). The variation of the wave impedance of the frozen soil was analyzed, and using viscoelastic theory, it was concluded that the increase in the wave impedance over short times was the result of unfrozen water relaxation in the frozen soil. The frozen soil was assumed to be composed of soil, ice, and water. The mesoscopic parameter (microcrack density) was related to the macroscopic physical quantity (wave velocity) through the effective medium theory neglecting crack interactions, and the longitudinal wave velocity was selected as the damage variable. The effects of the low-frequency parameters in the ZWT model were evaluated when applied to frozen soil. Under impact-loading conditions, with the initiation and expansion of internal microcracks, the low-frequency parameters lost their functions rather than degenerating into a spring and continued to contribute to the macroscopic mechanical properties of the frozen soil. Finally, a dynamic constitutive model of the frozen soil was established by including damage in the improved ZWT model. The theoretical curves obtained using the model were in good agreement with the experimental curves. The damage variable was physically significant, and the model could better reveal the damage mechanism of the frozen soil under impact loading.

2. Experiments and results

2.1. Dynamic uniaxial impact loading experiment of frozen soil

The dry density of the clay used in the experiment was 1.6 g/cm^3, and the granule distribution is shown in Table 1. The mass and moisture content of each specimen were 26.455 g and 30%, respectively. Each specimen with dimensions of Ø30 mm × 18 mm was compacted in a steel mold, after which it was placed into a cryostat cabinet and frozen for 24 h. It was subsequently quickly transferred to the SHPB device to complete the dynamic testing (Cao et al., 2018). Owing to the short test duration (100–200 μs), the behavior of the frozen soil was not affected by the environmental temperature.

The dynamic compressive deformation of the frozen soil was tested using a variable cross-section SHPB (Chen et al., 2017, 2018; Ma et al., 2017). When characterizing the dynamic mechanical response of the frozen soil at a high strain rate, a certain specimen size of the frozen soil is required to produce a meaningful representative volume (Chen and Song, 2010). Therefore, the specimen sizes were selected as Ø30mm × 18 mm. For the SHPB device to be suitable for the selected specimen sizes, the incident bar of the SHPB was converted to a variable cross-section bar. A schematic diagram of the experimental device is shown in Fig. 1. The device consisted of loading, bar, data acquisition, and recording systems. The bar material was a 7075-T6 aluminum alloy with a low wave impedance, and its elastic modulus was 75.8 GPa. The longitudinal wave velocity was 5200 m/s.

Table 1
Particle mixture ratios of original soil.

Particle size (mm)	2–0.85	0.85–0.425	0.425–0.18	<0.18
Weight fraction (%)	25.97	26.62	21.21	26.20

The direct loading of the cylindrical striker generated rectangular pulses in the bars. For materials with low wave impedances, a rectangular pulse creates two issues. (i) High-frequency oscillations are generated at the front of the pulse, resulting in oscillations of the actual stress in the specimen, which is equivalent to small loading and unloading values of the specimen. The instantaneous loading and unloading increase the strain during the stress oscillation, which is more significant for frozen soil with a low wave impedance. (ii) The stress balance during the experiment cannot be guaranteed owing to the low wave velocity of the frozen soil, and the validity of experimental data is affected. In a study of rocks (Li et al., 2015), a loading pulse in the form of a half-sine was used to solve these two issues. In this study, a red copper cylinder with dimensions of Ø6 mm × 1 mm was used as the pulse shaper, and the generated half-sine loading pulse is shown in Fig. 2. A two-wave method was adopted for data processing (Kim et al., 2019), expressed as follows:

$$\begin{cases} \dot{\varepsilon}(t) = -\frac{2C_b}{l_s}\varepsilon_r \\ \varepsilon(t) = -\frac{2C_b}{l_s}\int_0^t \varepsilon_r dt \\ \sigma(t) = \frac{A}{A_s}E_b\varepsilon_t \end{cases} \quad (1)$$

where C_b is the longitudinal wave velocity of the bar, ε_r and ε_t are the reflected and transmitted pulses, respectively, $\dot{\varepsilon}$ is the average strain rate, ε and σ are the calculated strain and stress, respectively, A and E_b are the cross-sectional area and elastic modulus of the bar, respectively, and l_s and A_s are the length and cross-sectional area of the specimen, respectively.

The test temperatures were −10, −15, and −20 °C, and the strain rate range was between 400 and 950 s^{-1}. The stress–strain curves at the different temperatures and strain rates are shown in Fig. 3. The failed specimens after the testing are shown in Fig. 4.

2.2. Analysis results after impact loading of frozen soil

2.2.1. Effects of temperature and strain rate on peak stress

The experimental stress–strain curves of the frozen soil at the same strain rate and different temperatures are shown in Fig. 5, and the peak stresses of the frozen soil at different temperatures and strain rates are shown in Fig. 6. From Figs. 5 and 6, it was concluded that the stress–strain curves of the frozen soil under impact loading mainly showed rate and temperature effects. The ice content of the frozen soil and the bonding strength between the soil and ice particles increased with a decrease in temperature, and the elastic modulus of the ice was more than one order of magnitude larger than that of the soil, leading to an increased strength of the frozen soil. The damage behavior of the frozen soil was caused by the many microcracks generated. The microcracks exhibited a relatively stable growth process at relatively low strain rates (such as 415 s^{-1}). During the growth process, different microcracks interacted with each other and finally merged to form the main crack. The macroscopic manifestation was fracture. At relatively high strain rates (such as 907 s^{-1}), many microcracks were activated in a short time. With the rapid propagation of the microcracks, the cracks did not have sufficient time to merge, and the macroscopic manifestation was fragmentation, which could bear high stresses.

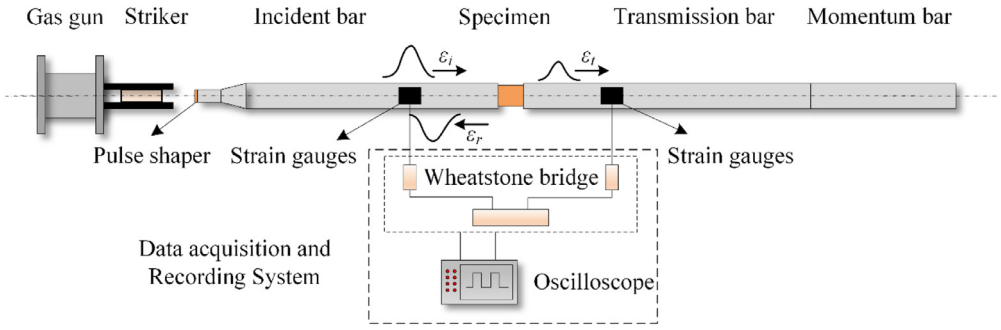

Fig. 1. SHPB device.

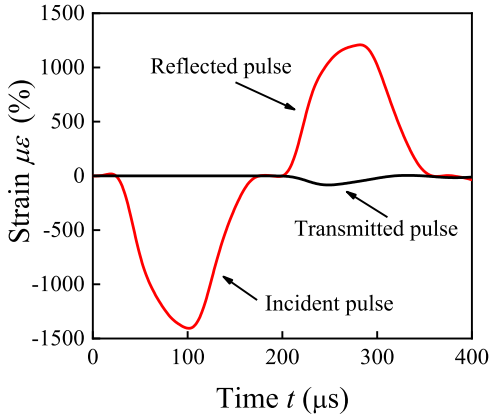

Fig. 2. Incident, reflected, and transmitted pulses in a pulse-shaped SHPB experiment.

2.2.2. Damage behavior of frozen soil under dynamic impact loading and influence of fluid on damage behavior

Frozen soil is composed of soil, ice, water, and air, and it contains many microcracks and other defects. The mechanical properties of frozen soil are affected by the soil type, temperature, moisture content, external loading type, and other factors. Because the fracture strength of the ice was significantly lower than that of the soil particles, during the deformation process of the frozen soil, microcracks were mainly generated at the contact point (surface) between the ice and soil particles or within the ice crystals. As shown in Fig. 4, the failure behaviors of the frozen soil exhibited characteristics typical of brittle materials. Brace and Martin III (1968) first proposed a sliding crack model to describe the failure behaviors of brittle materials under uniaxial loading. Many scholars have improved this model and applied it to the study of other brittle materials (Bischoff and Perry, 1991; Nemat-Nasser and Horii, 1982; Zhang and Zhao, 2014). The sliding crack model under uniaxial compression is shown in Fig. 7. In this model, the initial crack surface forms a random angle with the principal stress axis. With an increase in the loading, the tensile stress is concentrated at the tip of the crack due to the local shear stress. Once the critical stress level is reached, the crack begins to propagate. The direction of crack propagation is first perpendicular to the crack end and is finally parallel to the principal stress axis.

Under quasi-static loading, the fluid in the crack has sufficient time to flow into the crack tip. Meanwhile, there is a siphon effect at the crack tip, which can lubricate the crack contact surface and promote the crack propagation (Fig. 7). However, under impact loading, resistance at the stretch zone of the crack tip is generated due to the Stefan effect, and the saturated crack can be considered to be in an undrained state (Li, X., 2014). During the Stefan effect, two parallel plates are separated by a viscous liquid. When the plates are separated at a relative velocity v, a reaction force F is generated that resists the plate separation (Freund, 1998) (Fig. 8). The presence of the Stefan effect indicated that the saturated cracks were incompressible, which improved the strength of the frozen soil.

3. Constitutive damage model of frozen soil

3.1. Effective medium theory

The concept behind the effective medium theory is that a multiphase medium can be considered to be meso-inhomogeneous and macro-statistically homogeneous and that a representative volume element (RVE) can sufficiently represent the fine and microscopic characteristics of the medium (David et al., 1990). Among the many effective medium methods, the simplest and most effective one is the non-interactive assumption theory (NIA). In NIA theory, there are no stress interactions between the cracks and they are statistically complementary. In this study, cracks in the frozen soil were regarded as saturated coin-shaped cracks (Fig. 9).

In an RVE of frozen soil, cracks are regarded as a source of additional strain, and the strain of the frozen soil can be represented as follows (Grechka and Kachanov, 2006):

$$\varepsilon_{ij} = S_{ijkl}\sigma_{kl} = (S^0_{ijkl} + \Delta S_{ijkl})\sigma_{kl} = \varepsilon^0_{ij} + \Delta\varepsilon_{ij} \tag{2}$$

where S_{ijkl} are the effective compliances, S^0_{ijkl} are the matrix material (without cracks) compliances, ΔS_{ijkl} are the additional compliances caused by the cracks, and σ_{kl} are the applied stresses.

According to NIA theory, the extra compliance for the general case of nonrandom crack orientation is (Kachanov, 1980)

$$\Delta S_{ijkl} = h\left[\frac{1}{4}(\delta_{ik}\alpha_{jl} + \delta_{il}\alpha_{jk} + \delta_{jk}\alpha_{il} + \delta_{jl}\alpha_{ik}) + \psi\beta_{ijkl}\right] \tag{3}$$

Where $h = \frac{32(1-\nu^2)}{3(2-\nu)E}$, and E and ν are the elastic modulus and Poisson's ratio of the matrix material, respectively.

The second and fourth rank density tensors are defined as follows:

$$\begin{cases} \alpha_{ij} = \rho_c\langle n_i n_j\rangle \\ \beta_{ijkl} = \rho_c\langle n_i n_j n_k n_l\rangle \\ \rho_c = \frac{Nc^3}{V} \end{cases} \tag{4}$$

where α_{ij} and β_{ijkl} are the second and fourth rank crack density tensors, respectively, ρ_c is a scalar crack density parameter, N is the total number of cracks in a representative volume element V, and $\langle n_i n_j\rangle$ and $\langle n_i n_j n_k n_l\rangle$ represent the second and fourth rank moments of the crack direction distribution function, respectively. The angle brackets represent the statistical angular averages in a representative volume element RVE, defined as follows:

$$\langle n_i\rangle = \frac{1}{2\pi}\int_0^{2\pi} d\phi \int_0^{\pi/2} f(\theta, \phi)\sin\theta d\theta \tag{5}$$

where $f(\theta, \phi)$ is the crack direction distribution function.

ψ is related to the parameter δ_f (Schubnel and Guéguen, 2003) as follows:

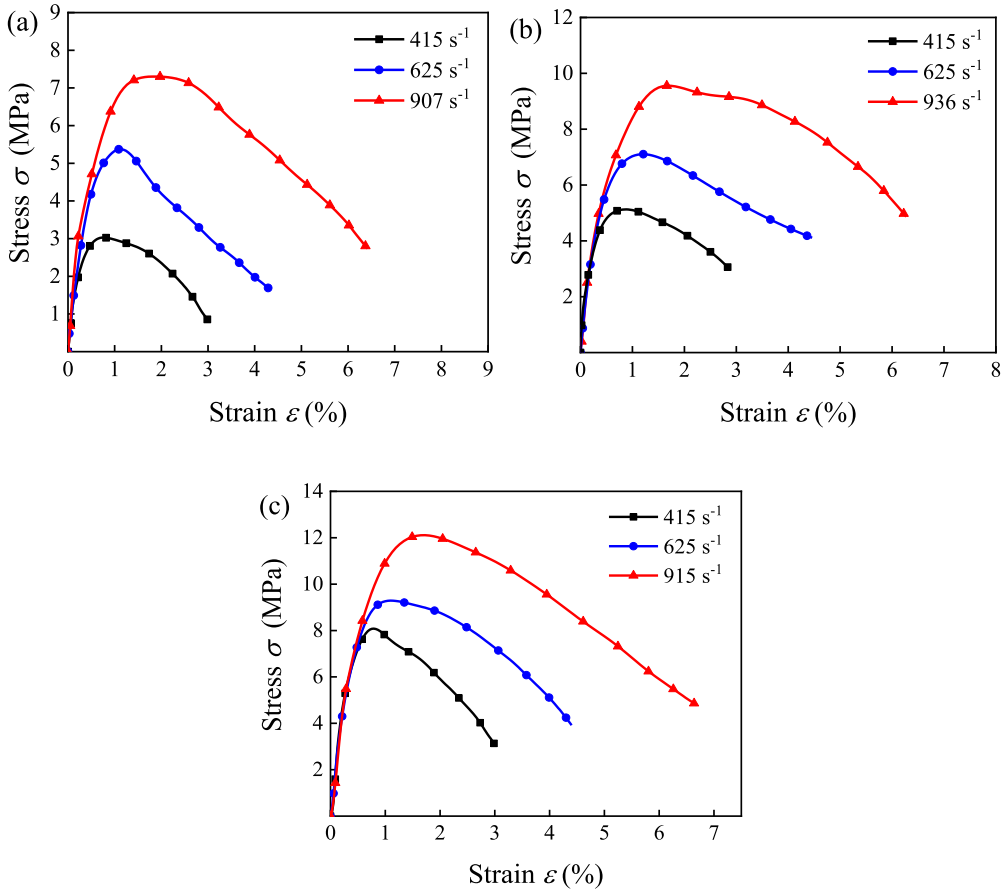

Fig. 3. Experimental stress–strain curves: (a) $T = -10$ ℃, (b) $T = -15$ ℃, and (c) $T = -20$ ℃.

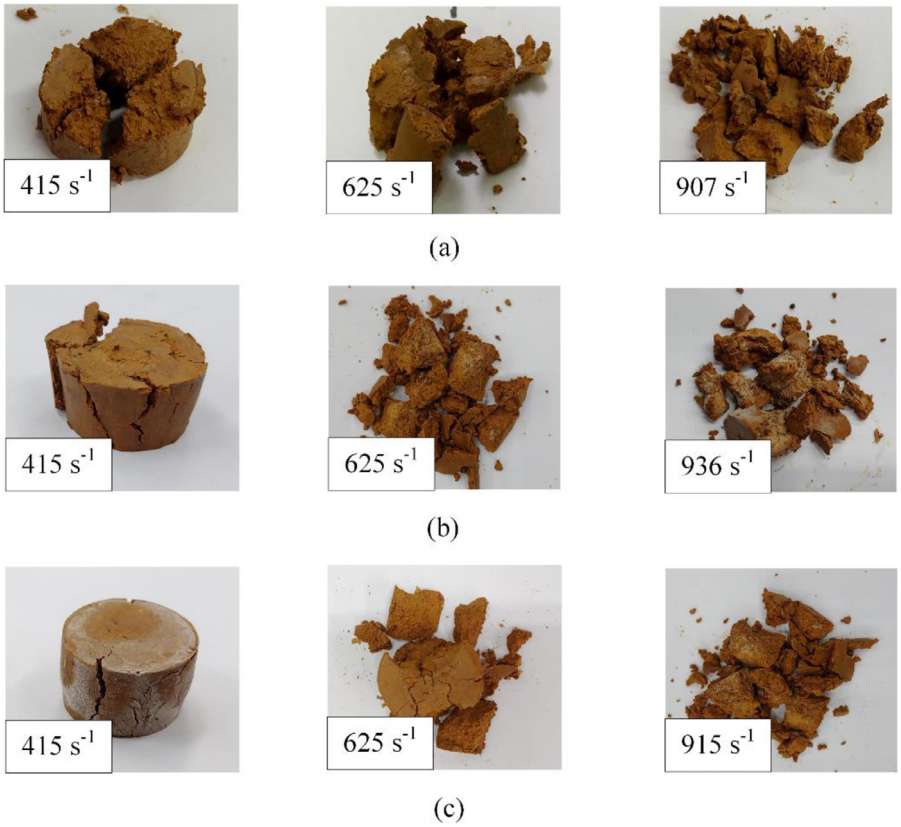

Fig. 4. Typical frozen soil specimens after testing: (a) $T = -10$ ℃, (b) $T = -15$ ℃, and (c) $T = -20$ ℃.

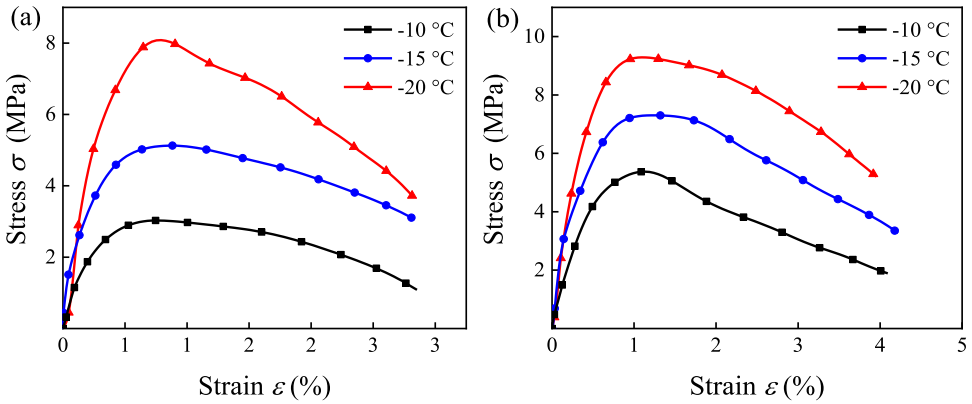

Fig. 5. Experimental curves of frozen soil at the same strain rate and different temperatures: (a)$\dot{\varepsilon} = 415\ s^{-1}$ and (b) $\dot{\varepsilon} = 625\ s^{-1}$.

$$\psi = \left(1 - \frac{v}{2}\right)\frac{\delta_f}{1 + \delta_f} - 1 \tag{6}$$

$$\delta_f = \frac{9\pi(1 - 2v)K}{16(1 - v^2)K_f}\zeta \tag{7}$$

where δ_f, which depends on the crack aspect ratio ζ, fluid bulk modulus K_f, and bulk modulus K of the frozen soil matrix, represents the relationship between the stress and fluid pressure.

When the frozen soil is subjected to uniaxial loading, as the stress increases, cracks are generated by friction sliding of the original cracks, and the propagation direction of the cracks is eventually parallel to the loading direction. Using the effective medium theory, cracks in frozen soil can be divided into two categories: cracks that are present in the original frozen soil, called random microcracks, and cracks with propagating directions parallel to the loading direction (z-axis, Fig. 9), called vertical microcracks. Considering a medium with these two kinds of cracks, the elastic potential energy can be written as:

$$f = f_0 + \Delta f_i + \Delta f_v \tag{8}$$

where f_0 is the elastic potential energy generated by matrix deformation, Δf_i , which depends on the random microcrack density ρ_r and the crack aspect ratio ζ_r, is the additional elastic potential energy caused by random cracks, and Δf_v, which depends on the vertical microcrack density ρ_v and the crack aspect ratio ζ_v, is the additional elastic potential energy due to vertical cracks. According to NIA theory, the effective compliances of a medium with two cracks under loading can be written as follows (Fortin et al., 2011):

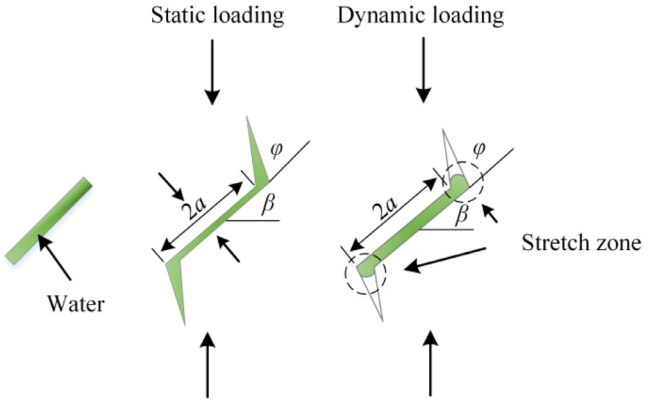

Fig. 7. Schematic diagram of saturated crack propagation.

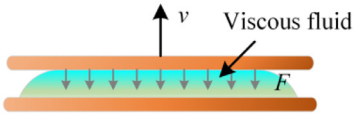

Fig. 8. Stefan effect under uniaxial loading.

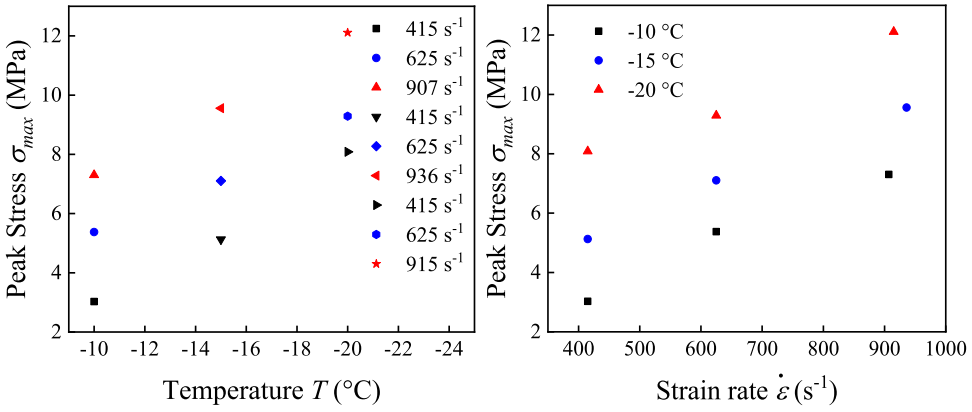

Fig. 6. Peak stresses of frozen soil.

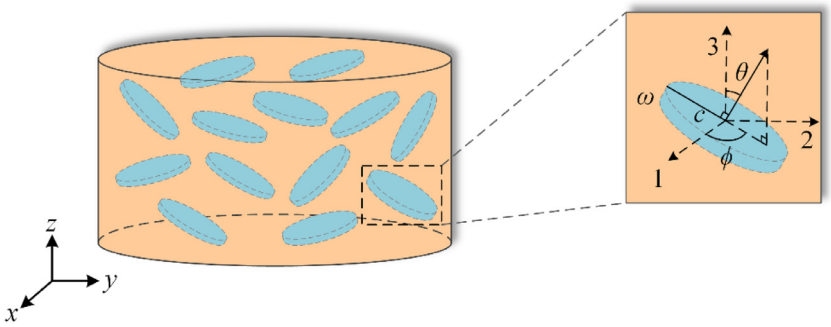

Fig. 9. Schematic diagram of saturated coin-shaped cracks, where c is the crack radius, ω is the crack width, and $\zeta = \omega/c$ is the crack aspect ratio.

$$\begin{cases} S_{11} = S_{22} = \frac{1}{E} + \rho_r \frac{h}{3}\left(1 + \frac{3}{5}\psi_r\right) + \rho_v \frac{h}{2}\left(1 + \frac{3}{4}\psi_v\right) \\ S_{12} = -\frac{v}{E} + \rho_r \frac{h}{15}\psi_r + \rho_v \frac{h}{8}\psi_v \\ S_{13} = S_{23} = -\frac{v}{E} + \rho_r \frac{h}{15}\psi_r \\ S_{33} = \frac{1}{E} + \rho_r \frac{h}{3}\left(1 + \frac{3}{5}\psi_r\right) \\ S_{44} = \frac{1}{G} + \rho_r h \frac{2}{3}\left(1 + \frac{3}{5}\psi_r\right) + \rho_v \frac{h}{2} \\ S_{66} = 2(S_{11} - S_{12}) \end{cases} \tag{9}$$

Where G is the shear modulus of a frozen soil matrix without cracks, and ψ_r and ψ_v, which can be calculated using Eq. (6), are parameters related to the random and vertical cracks, respectively.

3.2. Definition of damage variable

Damage refers to the process in which changes of a material's microstructure gradually accumulate, deteriorate its overall performance, and finally lead to its destruction under a certain loading and environment. Many scholars have studied the damage behaviors of frozen soil. Definitions of the damage variable have included the elastic modulus, the microscopic CT numbers, the effective ice content, and a random statistical damage model. We use the damage variable defined by the longitudinal wave velocity (Lemaitre, 1984; Yin et al., 2018):

$$D = 1 - \left(\frac{\tilde{V}_p}{V_p}\right)^2 \tag{10}$$

where V_p and $\tilde{V}_p$ are the longitudinal wave velocity of the frozen soil in the non-damaged and damaged states, respectively.

The wave velocity of a damaged medium containing cracks is a function of its propagation angle (Mavko et al., 2009):

$$\begin{cases} V_p(\gamma) = (C_{11}\sin^2\gamma + C_{33}\cos^2\gamma + C_{44} + \sqrt{M})^{\frac{1}{2}}(2\rho)^{-\frac{1}{2}} \\ M = [(C_{11} - C_{44})\sin^2\gamma - (C_{33} - C_{44})\cos^2\gamma]^2 + (C_{13} + C_{44})^2\sin^2 2\gamma \end{cases} \tag{11}$$

where $C_{ij}(i, j = 1, 2, 3, ...,6)$ are the elastic constants, calculated by the relationship $\mathbf{C}=\mathbf{S}^{-1}$, and γ is the angle between the wave propagation and loading directions.

Fig. 10 shows the variation of $V_P(\gamma)/V_P(0)$ with the angle γ based on Eq. (11). The elastic wave velocity changes most when the propagation direction is vertical to the loading direction. The elastic wave velocity in damaged materials is most sensitive to vertical cracks, which are propagated along the loading direction (Crampin, 1981), and better reflect the propagation of cracks. In this paper, $\tilde{V}_p$ in Eq. (10) is replaced by V_{P90}, which is the longitudinal wave velocity perpendicular to the loading direction:

$$D = 1 - \left(\frac{V_{p90}}{V_{p0}}\right)^2 \tag{12}$$

Substituting Eq. (11) into Eq. (12) yields the following relationship:

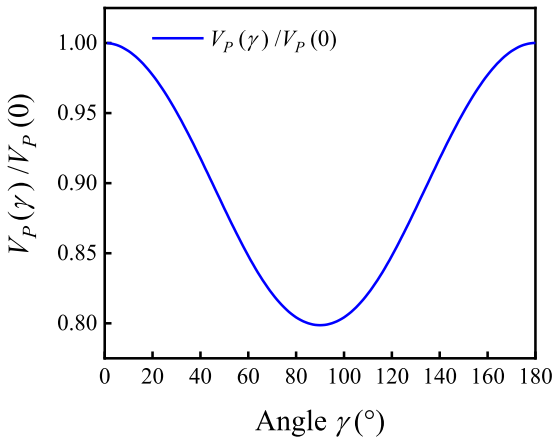

Fig. 10. Variation of $V_P(\gamma)/V_P(0)$ with angle γ.

$$D = 1 - \frac{C'_{11}}{C_{33}} \tag{13}$$

where the angular index is the stiffness constant after loading.

3.3. Dynamic constitutive model

Frozen soil is a type of rate-dependent material, and its mesoscopic components have different response characteristics under high strain rates. According to stress-wave theory (Wang, 2005), the response can be generally divided into two parts: a time-independent transient response and a time-dependent non-transient response, where the non-transient response is the viscoelastic response caused by the viscous dissipation force inside the material. Tang et al. proposed the ZWT model, which is a dynamic constitutive model capable of describing the nonlinear viscoelastic responses of materials (Fig. 11) (Wang, 2003). This model has been widely used as the dynamic constitutive model of

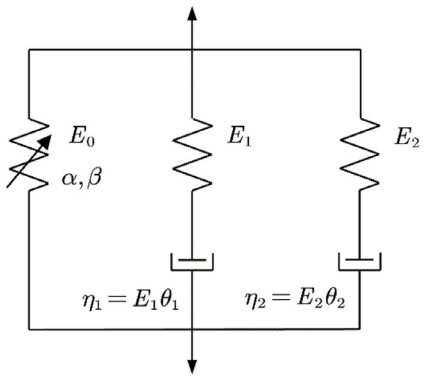

Fig. 11. ZWT nonlinear viscoelastic model.

many materials (Dong et al., 2018; Zhang et al., 2016). The formulation of the ZWT model can be expressed as follows:

$$\sigma = E_0\varepsilon + \alpha\varepsilon^2 + \beta\varepsilon^3 + E_1\int_0^t \dot{\varepsilon}(\tau)\exp\left(-\frac{t-\tau}{\theta_1}\right)d\tau + E_2\int_0^t \dot{\varepsilon}(\tau)\exp\left(-\frac{t-\tau}{\theta_2}\right)d\tau \quad (14)$$

The model consists of a nonlinear spring and two Maxwell elements with different relaxation times. The first three terms describe the equilibrium response of the nonlinear spring and represent the mechanical properties of the materials under quasi-static loading. E_0, α, and β are the corresponding elastic constants. The middle integral term describes the viscoelastic response under low strain rates. E_1 and θ_1 are the elastic constant and relaxation time of the corresponding Maxwell element, respectively. The final integral term describes the viscoelastic response under a high strain rate. E_2 and θ_2 are the elastic constant and relaxation time of the corresponding Maxwell element, respectively. Under impact loading, for materials without damage behaviors (such as polymer materials (Jiang et al., 2016)), the low-frequency Maxwell element with relaxation time θ_1 (10^0–10^2 s) will degenerate into a simple spring because there is not sufficient time for relaxation to occur. The responses of materials with high strain rates are described by the high-frequency Maxwell element with relaxation time θ_2 (10^{-6}–10^{-4} s).

The purpose of this model is to describe the impact deformation behavior of a material without damage. For frozen soil, the dynamic parameters of the high- and low-frequency elements in Eq. (14) are determined by the resonance column method (deformation in the range of 10^{-6}–10^{-3}%) and the dynamic triaxial method (deformation in the range of 10^{-3}–10^{-1}%), respectively. In this strain range, the frozen soil does not exhibit damage behaviors, such as microcrack propagation, and the bonds between the soil and ice are not damaged. However, under a large impact deformation (deformation in the range of 3–10%) of the frozen soil, microcracks are generated within ice crystals and at the interfaces between the soil and ice (Qi and Ma, 2010). With the propagation of microcracks, the bonds between the soil and ice within the frozen soil are destroyed rapidly. The Maxell element with low-frequency parameters lost its function rather than degenerating into a simple spring and continues to contribute to the macroscopic mechanical properties of the frozen soil. Therefore, the influence of the first integral term in Eq. (14) can be ignored.

Under quasi-static loading, the elastic section of the uniaxial stress–strain curve of the frozen soil is linear (Zhu et al., 1992), and the nonlinear spring in Eq. (14) can be considered to be linear. Thus, the constitutive equation is simplified to:

$$\begin{cases}\sigma = (1-D)\left(E_0\varepsilon + E_2\int_0^t \dot{\varepsilon}(\tau)\exp\left(-\frac{t-\tau}{\theta_2}\right)d\tau\right)\\ D = 1 - \frac{C_{11}'}{C_{33}}\end{cases} \quad (15)$$

3.4. Random microcrack density ρ_r

The wave impedance of the frozen soil, calculated by the product of the density and the longitudinal wave velocity, represents the stress wave propagation and reflection in the frozen soil. Because the longitudinal wave velocity is highly sensitive to the microstructure of the frozen soil, it reflects the changes of the microcracks. When the strain value is very small, the change of the density of the frozen soil can be neglected, and thus, the change of the wave impedance can represent the propagation of microcracks in the frozen soil.

When the stress wave propagates from one medium to another, due to a mismatch of the wave impedance properties, the incident pulse transmits and reflects at the interface of the two media, as shown in Fig. 12. The left and right regions in Fig. 12 are the incident and transmission bars of the SHPB experimental device, respectively, where the wave impedance is $\rho_b C_b$. The middle region represents the specimen, where the wave impedance is ρC. A_1 represents the contact surface between the incident bar and the specimen, A_2 represents the contact surface between the specimen and the transmission bar, and σ_I, σ_R, and σ_T are the incident, reflection, and transmission stresses, respectively.

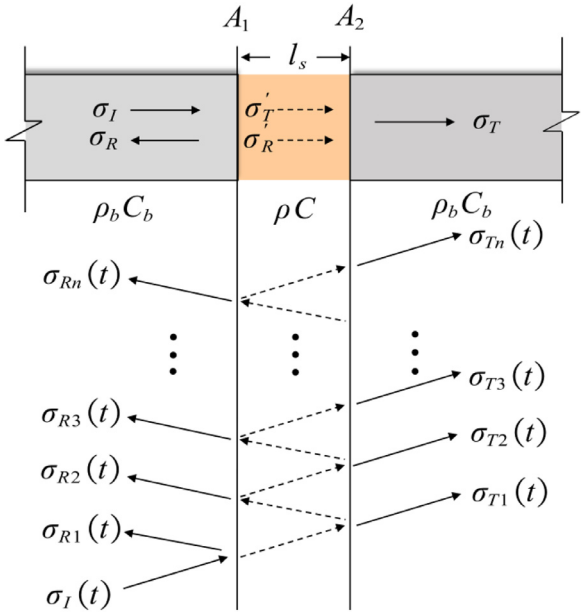

Fig. 12. Propagation diagram of transmission and reflection on SHPB.

From Jin et al. (2011), based on one-dimensional stress wave theory, the wave impedance can be expressed by the incident and transmitted pulses in the impact process as follows:

$$\begin{cases}\rho_b C_b = \frac{2-n(t)-2\sqrt{1-n(t)}}{n(t)}\rho C\\ n(t) = \frac{\sigma_T(t)}{\sigma_I(t)}\end{cases} \quad (16)$$

where σ_I and σ_T, which are calculated using values of the incident and transmitted pulses within the respective sampling time $0 \le t \le 2l_s/C$, denote the incident and transmitted stresses, respectively. The length of the specimen was 18 mm, and the longitudinal wave velocity was 2000m/s . Therefore, the time range between 0 and 9 μs was adequate to detect the entire elastic wave for the selected temperature. Fig. 13 shows the wave impedance variation of the frozen soil calculated using Eq. (16) when the temperature was -10 ˚C and the strain rate was 936

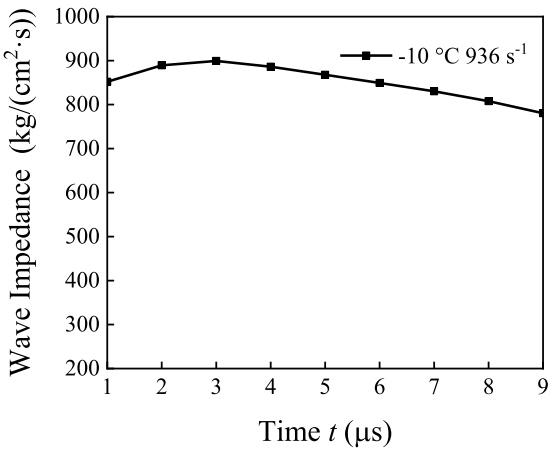

Fig. 13. Variation of wave impedance with time.

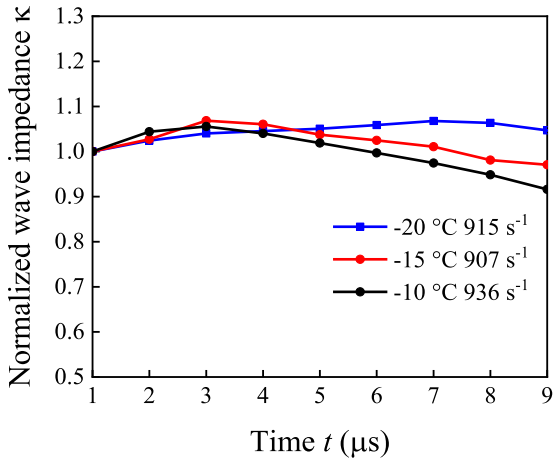

Fig. 14. Variation of normalized wave impedance κ with time.

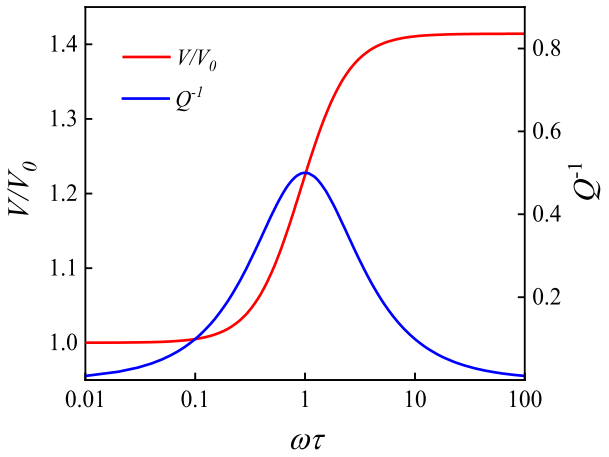

Fig. 15. Variation of the dimensionless phase velocity $V/V_0$and the dimensionless attenuation factor Q^{-1} with $\omega\tau$.

s^{-1}. The normalized wave impedance κ was introduced to allow dimensionless comparative analysis:

$$\kappa = \frac{\rho C(t)}{\rho C(1)} \tag{17}$$

where $\rho C(1)$ is the wave impedance value calculated when $t = 1$ μs.

Fig. 14 shows the variation of the normalized wave impedance κ. The wave impedance of the frozen soil increased until approximately 3 μs. Jin et al. (2011) analyzed the variation of the wave impedance of sandstone during impact loading, which increased until approximately 15 μs. They concluded that this phenomenon was caused by the compaction of the pores in sandstone. However, the wave impedance in the frozen soil increased until only approximately 3 μs, and the strain produced was on the order of 10^{-5}, which could not cause pore compaction. Thus, this phenomenon was caused by different mechanisms of stress wave propagation in the frozen soil.

According to viscoelastic theory, the constitutive equation of the ZWT model can be written as:

$$\sigma + \tau\dot{\sigma} = M_0\varepsilon + \tau M_\infty\dot{\varepsilon} \tag{18}$$

where M_0, calculated by the sum of E_0 and E_1, is called the unrelaxed modulus; M_∞, calculated by the sum of E_0, E_1, and E_2, is called the relaxation modulus; $\tau = \eta/E_2$ is the relaxation time; and η is the viscosity coefficient of the material.

The stress and strain forms were assumed to be sinusoidal (Christensen, 2012), $\sigma = \sigma_0 e^{i\omega t}$ and $\varepsilon = \varepsilon_0^{i(\omega t-\varphi)}$, where ω is the circular frequency. By substituting this form into Eq. (18), we obtain $\sigma = \tilde{M}\varepsilon$, where $\tilde{M} = M_\infty + \frac{M_0 - M_\infty}{1 + i\omega\tau}$ is the complex modulus of the frequency dependence. The wave velocity can be obtained from the relation $V = \sqrt{\mathrm{Re}[\tilde{M}]/\rho}$. When$\omega \to \infty$, $\tilde{M} = M_\infty$ and $V = \sqrt{M_\infty/\rho}$. When $\omega \to 0$, $\tilde{M} = M_0$ and $V = \sqrt{M_0/\rho}$.

The dimensionless attenuation factor Q^{-1} can be obtained as follows:

$$Q^{-1} = \frac{\mathrm{Im}[\tilde{M}]}{\mathrm{Re}[\tilde{M}]} = \frac{(M_\infty - M_0)}{\sqrt{M_0 M_\infty}} \frac{\omega\tau}{\sqrt{\frac{M_0}{M_\infty}} + \sqrt{\frac{M_0}{M_\infty}}(\omega\tau)^2} \tag{19}$$

Based on Eq. (19), the dimensionless attenuation factor Q^{-1} has a maximum value when $\omega\tau = 1$. Fig. 15 shows the results of the dimensionless phase velocity V/V_0 and the dimensionless attenuation factor Q^{-1} with respect to $\omega\tau$, where E_2 is equal to $E_0 + E_1$ and $V_0 = \sqrt{M_0/\rho}$.

As shown in Fig. 15, the dimensionless phase velocity changes significantly at $\omega\tau = 1$. According to Biot theory, a dispersion phenomenon occurs when an elastic wave propagates in saturated porous media (Guéguen et al., 2004), which depends on the local flow caused by the strain frequency received by the medium. When the elastic wave propagates in the medium, a pressure difference occurs between adjacent cracks. When the frequency is higher than the critical frequency, it is impossible for the pores of adjacent cracks to reach equilibrium in a very short time. In other words, there is not significant fluid flow between the RVE and the adjacent environment. The critical frequency is defined as $f_c = \zeta^3 E/20\eta$ (Le Ravalec and Guéguen, 1996). If the elastic modulus of the frozen soil is 1 GPa and the viscosity coefficient of the fluid is 10^{-3} Pa•s, the calculated critical frequency is 50 kHz. Based on the relationship between the circular frequency and relaxation time $\omega\tau = 1$, the relaxation time calculated from the critical frequency is about 3 μs. Under impact-loading conditions, the propagation of the stress waves in frozen soil is accompanied by the relaxation of unfrozen water. Thus, there was not significant fluid flow between the microcracks, and the unfrozen water in the microcracks was not squeezed out. The wave impedance of the frozen soil increased in a very short time (3 μs), and the dynamic mechanical properties of frozen soil improved. In this paper, random microcracks were assumed to be fluid saturated, and the random microcrack density can be calculated as the volume fraction of the unfrozen water.

3.5. Vertical microcrack density ρ_v

The crack nucleation rate of the impact loading is assumed to follow the double parameter Weibull function (Taylor et al., 1985):

$$N(\varepsilon) = k\varepsilon^m \tag{20}$$

where N is the number of cracks under a strain ε, k and m are related to the material properties. Substitute Eq. (20) into Eq. (4) yields the vertical microcrack density:

$$\rho_v = k\varepsilon^m c^3 \tag{21}$$

where c is the average size of the crack, as determined by the expression (Grady and Kipp, 1980):

$$c = \left(\frac{\sqrt{20}K_{IC}}{\rho C\dot{\theta}_{\max}}\right)^{2/3} \tag{22}$$

where K_{IC} is the dynamic fracture toughness of the frozen soil, C is the longitudinal wave velocity of the material, and $\dot{\theta}_{\max}$ is the maximum volumetric strain rate of the material failure.

3.6. Static elastic modulus

In a previous study (Zhu et al., 2010), the law of mixtures was used to evaluate the quasi-static elastic modulus and the Poisson's ratio of the frozen soil:

$$\begin{cases} E_0 = \dfrac{[f_s E_s(1-2v_i)+f_i E_i(1-2v_s)][f_s E_s(1+v_i)+f_i E_i(1+v_s)]}{f_i E_s(1+v_i)(1-2v_s)} \\ v_0 = \dfrac{f_s E_s v_s(1+v_i)(1-2v_i)+f_i E_i v_i(1+v_s)(1-2v_s)}{f_s E_s(1+v_i)(1-2v_i)+f_i E_i(1+v_s)(1-2v_s)} \end{cases} \tag{23}$$

where f_s and f_i are the volume fraction of the soil and ice, respectively, E_s and E_i are the elastic moduli of the soil and ice, respectively, and v_s and v_i are the Poisson's ratios of the soil and ice, respectively.

Because there is always some unfrozen water in the negative temperature range of artificial polycrystalline ice (Wen et al., 2012), the response of the unfrozen water should be included in the compression behavior of the ice under quasi-static loading. Thus, f_i in Eq. (23) should be modified to $f_i + f_w$, and Eq. (23) can be rewritten as:

$$\begin{cases} E_0 = \dfrac{[f_s E_s(1-2v_i)+(f_i+f_w)E_i(1-2v_s)][f_s E_s(1+v_i)+(f_i+f_w)E_i(1+v_s)]}{(f_i+f_w)E_s(1+v_i)(1-2v_s)} \\ v_0 = \dfrac{f_s E_s v_s(1+v_i)(1-2v_i)+(f_i+f_w)E_i v_i(1+v_s)(1-2v_s)}{f_s E_s(1+v_i)(1-2v_i)+(f_i+f_w)E_i(1+v_s)(1-2v_s)} \end{cases} \tag{24}$$

where f_w is the volume fraction of the unfrozen water.

The unfrozen water content of the frozen soil at different temperatures was shown to depend on the temperature as follows (Zhang et al., 2018):

$$W_u = AT^B \tag{25}$$

where T is the absolute value of the temperature, and A and B, which are related to soil type, are constants with values of 16.2 and -0.233 (Zhu et al., 2017), respectively. The volume fraction of each phase can be expressed as follows:

$$\begin{cases} f_w = \dfrac{AT^B m_s}{\rho_w V} \\ f_i = \dfrac{(W_0 - AT^B)m_s}{\rho_i V} \\ f_s = \dfrac{m_s}{\rho_s V} \\ V = V_s + V_w + V_i \end{cases} \tag{26}$$

where V_s, V_w, and V_i are the volumes of the soil particles, water, and ice particles, respectively, ρ_w and ρ_i are the density of the water and ice, respectively, ρ_s is the grain density of the soil, and W_0 is the initial moisture content.

3.7. Coupling coefficient of stress and fluid pressure ψ

The parameter ψ, which represents the relationship between the stress and fluid pressure in the frozen soil, depends on the Poisson's ratio v, the bulk modulus of the frozen soil matrix without cracks K, the bulk modulus of the fluid K_f, and the aspect ratio of the crack ζ. The crack aspect ratio ζ is 0.01 Li et al., 2004). K and v can be approximated from the dynamic triaxial tests of the frozen soil. In this strain range (10^{-3}–10^{-1}%), the microcracks in frozen soil do not propagate significantly, and the properties of frozen soil matrix (without cracks) can be represented approximately. The Poisson's ratio v was set to 0.35, and the bulk modulus K was approximately the same order of magnitude as the fluid bulk modulus K_f. Using Eqs. (6) and ((7), we determined that $\delta_f \ll 1$ and $\psi_r = -1$.

During the process of impact loading, the pore saturation in the microcracks changes with the propagation and nucleation of microcracks, which will affect the fluid bulk modulus K_f. The fluid bulk modulus K_f is calculated using the following equation (Bear, 1972):

$$K_f = \frac{1}{1/K_w + (1-S_r)/P_a} \tag{27}$$

where P_a is the absolute fluid pressure, which is equal to 150 kPa, and S_r is the pore saturation. Under impact loading, if the phase transition process and the compressibility of soil particles, ice particles, and water are neglected, the pore saturation S_r can be expressed as follows:

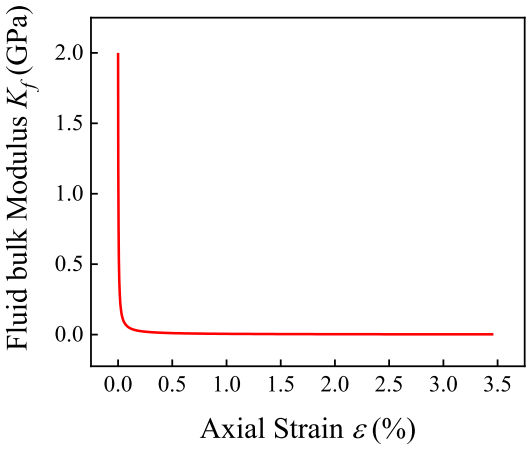

Fig. 16. Variation of the fluid bulk modulus K_f with the axial strainε.

$$S_r = \frac{V_w}{V_v} = \frac{1/\rho_w}{(1+\theta)(1/\rho_s + (W_0 - W_u)/\rho_i + W_u/\rho_w) - 1/\rho_s - (W_0 - W_u)/\rho_i} = \frac{W_u/\rho_w}{\theta/\rho_s + \theta(W_0 - W_u)/\rho_i + (1+\theta)W_u/\rho_w} \tag{28}$$

where θ is the volume strain, which is equal to $(1-2v_0)\varepsilon$, and V_w and V_v are the unfrozen water volume and microcrack volume, respectively.

Fig. 16 shows the relationship between the axial strain ε and the fluid bulk modulus K_f calculated using Eqs. (24)–(28) for a temperature of -10 ˚C and moisture content of 30%. The specific values of the parameters are shown in Table 2. The fluid bulk modulus K_f decreased rapidly with an increase in the strain. Therefore, using Eqs. (6) and (7), we determined that $K_f \ll E$, $\delta_f \gg 1$, and $\psi_v = -\frac{v}{2} = -0.175$.

4. Verification of constitutive model

The constitutive model proposed in this paper contains 13 parameters. The values of the water density ρ_w, grain density of the soil ρ_s, ice density ρ_i, Poisson's ratio of the soil v_s, and Poisson's ratio of the ice v_i are shown in Table 2 in Section 3.7. The longitudinal wave velocity C and the dynamic fracture toughness K_{IC} of the frozen soil are material constants that were determined through experiments. The static elastic modulus E_0 can be calculated using Eq. (23). The values of these parameters are shown in Table 3. Parameters k, m, E_2, and θ_2 were determined by least squares fitting of the experimental data. The values of these parameters are shown in Table 4. A comparison between the experimental and theoretical curves is shown in Fig. 17.

The contact conditions between the soil particles can be divided into three types (Hillel, 2012): (i) solid–solid (SS)—direct contact between soil particles, (ii) solid–liquid–solid (SLS)—soil particles are separated by water, and (iii) solid–solid–liquid–solid (SSLS)—some soil particles are in contact and others are separated by water. After freezing, more complex interfaces are formed. Fig. 19 shows the typical microstructure of the SLS and SS contact types under freezing conditions. In addition to the direct contact of the soil particles, cementation between the soil and ice and adhesion between the ice and water were evident. Moreover, the frozen soil was composed of soil particles of different sizes, and thus, the microstructure shown in Fig. 19 is multiscale. When the stress wave propagates in frozen soil, it is transmitted and reflected at the interfaces of the microstructure. These characteristics result in complex relaxation behavior in the frozen soil and lead to the dispersion of the

Table 2
Material parameters of frozen soil.

v_s	v_i	ρ_w/(g/(cm)^3)	ρ_s/(g/(cm)^3)	ρ_i/(g/(cm)^3)
0.3	0.33	1.0	2.65	0.92

Table 3
Material parameters in constitutive model.

T/°C	E_s/MPa	E_l/GPa	E_0/MPa	C/(m/s)	K_{IC}/(MPa·$\sqrt{m}$)
−10	40	0.559	277	2019	0.9
−15	40	1.06	507	2320	
−20	40	1.32	626	2352	

Table 4
Fit parameters of constitutive model.

T/°C	k	m	E_2/GPa	θ_2/μs
−10	2.32–2.56 × 10^8	2	1.06	5.6–6.9
−15	2.56–3.12 × 10^8	2	1.63	3.2–5.5
−20	2.96–3.20 × 10^8	2	1.92	3.6–6.0

frozen soil. Therefore, ranges of the parameters k and θ_2 in Table 4 were used.

As shown in Fig. 17, the theoretical curves calculated by the model agreed with the experimental curves, and the model could accurately reflect the temperature and strain rate effects in the frozen soil under impact loading. Because the damage variable has physical significance, the model can better reveal the damage and deformation mechanism of frozen soil under impact loading.

Fig. 18 shows the stress–strain and damage evolution curves of frozen soil at a temperature of -10 ˚C and the strain rate of 625 s^{-1}. Before the stress–strain curve reached the peak stress, the damage value increased rapidly due to the propagation of internal microcracks as the strain increased. After the peak stress, due to the propagation of microcracks, the integrity of the internal microstructure of the frozen soil continuously deteriorated, which led to a continuous decrease in the stress in the frozen soil.

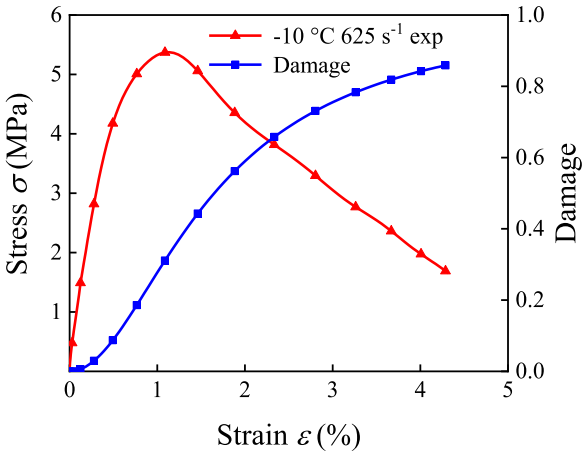

Fig. 18. Experimental and damage evolution curve at $T = -10$ ˚C and $\dot{\varepsilon} = 625s^{-1}$.

5. Conclusion

The dynamic mechanical properties of frozen soil at different temperatures (−10, −15, and −20 ˚C) and high strain rates (400–950 s^{-1}) were tested using a split Hopkinson pressure bar (SHPB). Based on the effective medium theory, the mesoscopic parameters (microcrack density) and macroscopic physical quantities (wave velocity) were connected. The ZWT model was improved based on the characteristics of the frozen soil. Finally, a dynamic constitutive model of the frozen soil with a longitudinal wave velocity as the damage variable was

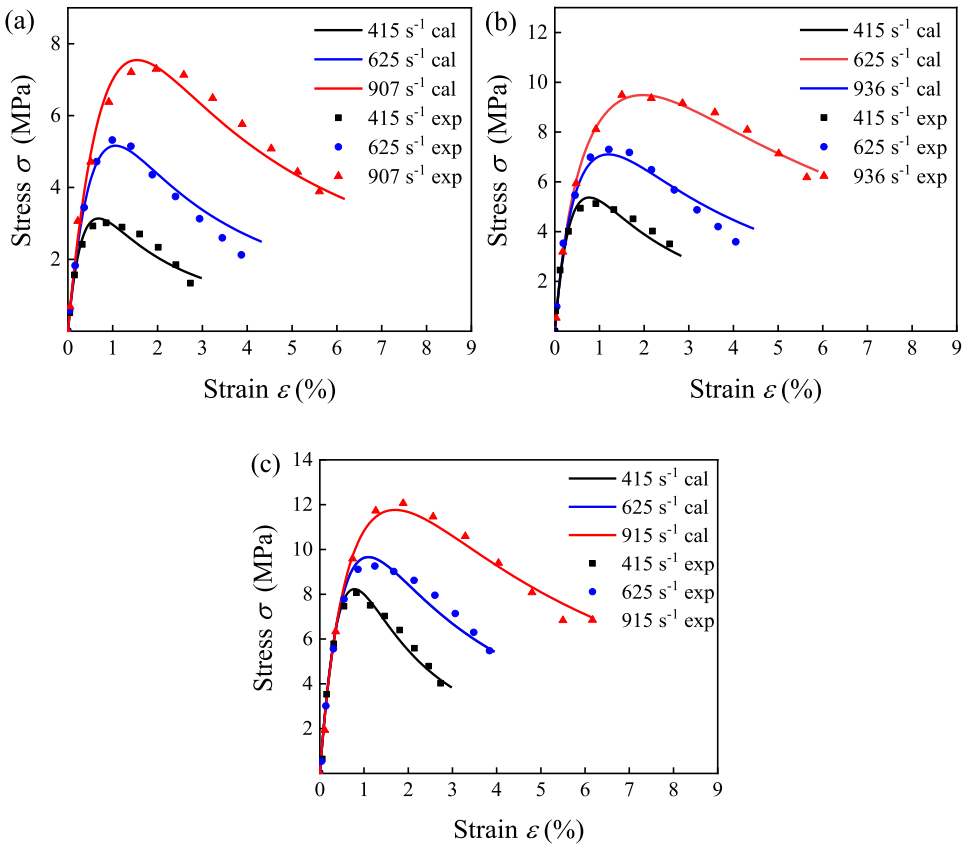

Fig. 17. Experimental and theoretical curves: (a) −10 ˚C, (b) −15 ˚C, and (c) −20 ˚C(cal and exp denote calculated and experimental values, respectively).

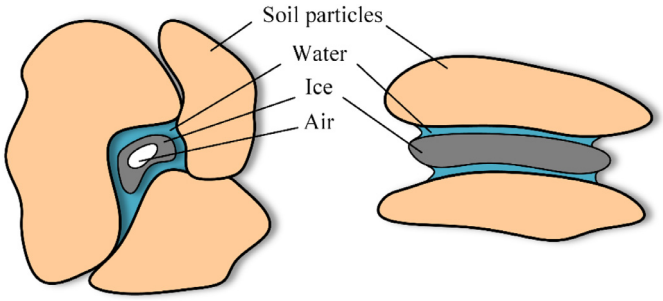

Fig. 19. Typical microstructure of the SLS and SS contact types under freezing conditions.

established. The conclusions of the study were as follows.

(1) Rate and temperature effects under impact loading occur in frozen soil. The peak stress increased with an increase in the strain rate and decreased with an increase in the temperature. The responses of the internal micro-defects to the strain rate of the frozen soil at different temperatures resulted in different macroscopic failure characteristics. Under low-strain-rate conditions, the microcracks underwent a relatively stable propagation process. During the propagation process, cracks interacted with each other and finally merged to form a main crack, which manifested as a fracture at the macroscopic scale. Under high-strain-rate conditions, a large number of microcracks were activated in a short time. With the rapid growth of these microcracks, the microcracks did not have sufficient time to merge into a main crack, and the macroscopic manifestation was fragmentation, which could bear relatively high stresses.
(2) According to the experimental data, the wave impedance of the frozen soil increased in a very short time during the loading process. This phenomenon was the result of unfrozen water relaxation in the frozen soil under high strain rates, as revealed through viscoelastic theory. Due to the Stefan effect in the process of wing crack growth under high-strain-rate loading, the fluid-saturated crack exhibited an “incompressible” characteristic under high strain rates. Under impact loading, the unfrozen water was one of the important factors that led to the increase in the peak stress of the frozen soil.
(3) The ZWT constitutive model revealed that under impact-loading conditions, low-frequency parameters affected the mechanical behavior of the frozen soil only under minimal strain. With the initiation and propagation of internal microcracks in the frozen soil, the Maxwell element that represented the low-frequency dynamic response of the material lost its function rather than degenerating into a simple spring, and thus, it continued to contribute to the macroscopic mechanical properties of the frozen soil.
(4) A constitutive model for the damage dynamics was proposed based on the damage variable defined using the longitudinal wave velocity. In engineering practice, the damage variable defined by the longitudinal wave velocity can be measured easily through ultrasonic nondestructive testing technology, and thus, it has high engineering application value.

Declaration of Competing Interest

We wish to confirm that there are no known conflict of interest associated with this publication and there has been no significant financial support for this work that could have influenced its outcome.

Acknowledgments

This work was supported by the National Key Research and Development Program of China [grant number 2016YFB1200505], the National Natural Science Foundation of China [grant numbers 11672253 and 11972028], and the Opening Foundation of the State Key Laboratory for Strength and Vibration of Mechanical Structures [grant number SV2019_KF-19].

References

Bear, J., 1972. Dynamics of Fluids in Porous Media. Elsevier, New York.
Bischoff, P.H., Perry, S.H., 1991. Compressive behaviour of concrete at high strain sates. Mater. Struct. 24 (6), 425–450.
Brace, W.F., Martin III, R.J., 1968. A test of the law of effective stress for crystalline rocks of low porosity. Int. J. Rock Mech. Min. 5, 415–426.
Cao, C., Zhu, Z., Fu, T., Liu, Z., 2018. A constitutive model for frozen soil based on rate-dependent damage evolution. Int. J. Damage Mech. 27 (10), 1589–1600.
Chen, W., Song, B., 2010. Split Hopkinson (Kolsky) bar design. Testing and Applications. Springer, New York.
Chen, X., Chen, C., Liu, Z., Lu, J., Fan, X., 2018. Compressive Behavior of Concrete under High Strain Rates after Freeze-thaw Cycles. Comput. Concrete. 21 (2), 209–217.
Chen, X., Xu, L., Zhu, Q., 2017. Mechanical Behavior and damage evolution for concrete subjected to multiple impact loading. Ksce J. Civ. Eng. 21 (6), 2351–2359.
Christensen, R., 2012. Theory of Viscoelasticity: An Introduction. Elsevier, New York.
Crampin, S., 1981. A review of wave motion in anisotropic and cracked elastic-media. Wave Motion 3 (4), 343–391.
David, C., Gueguen, Y., Pampoukis, G., 1990. Effective medium theory and network theory applied to the transport properties of rock. J. Geophys. Res. 95 (B5), 6993.
Dong, S., Han, B., Yu, X., Ou, J., 2018. Dynamic impact behaviors and constitutive model of super-fine stainless wire reinforced reactive powder concrete. Constr. Build. Mater. 184, 602–616.
Fortin, J., Stanchits, S., Vinciguerra, S., Guéguen, Y., 2011. Influence of thermal and mechanical cracks on permeability and elastic wave velocities in a basalt from Mt. Etna volcano subjected to elevated pressure. Tectonophysics. 503 (1-2), 60–74.
French, H.M., 2017. The Periglacial Environment. John Wiley & Sons, New Jersey.
Freund, L.B., 1998. Dynamic Fracture Mechanics. Cambridge University Press, New York.
Grady, D.E., Kipp, M.E., 1980. Continuum modelling of explosive fracture in oil shale. Int. J. Rock Mech. Min. Sci. Geomech. Abstr. 17 (6), 147–157.
Grechka, V., Kachanov, M., 2006. Effective elasticity of rocks with closely spaced and intersecting cracks. Geophysics 71 (3), D85–D91.
Guéguen, Y., Dormieux, L., Boutéca, M., 2004. Mechanics of Fluid-saturated Rocks. Academic Press, New York.
He, P., Cheng, G., Zhu, Y., 1999. Constitutive Theories on viscoelastoplasticity and damage of frozen soil. Sci. China-Earth Sci. 42 (1), 38–43.
Hillel, D., 2012. Applications of Soil Physics. Academic, New York.
Jiang, J., Xu, J., Zhang, Z., Chen, X., 2016. Rate-dependent compressive behavior of EPDM insulation: experimental and constitutive analysis. Mech. Mater. 96, 30–38.
Jin, J., Li, X., Yin, Z., Zou, Y., 2011. A method for defining rock damage variable by wave impedance under cyclic impact loadings. Chin. J. Rock Soil Mech. 5 (32), 1385–1410.
Kachanov, M., 1980. Continuum model of medium with cracks. J. Eng Mech Div. 106 (5), 1039–1051.
Kim, K., Lee, S., Cho, J., 2019. Effect of maximum coarse aggregate size on dynamic compressive strength of high-strength concrete. Int. J. Impact Eng. 125, 107–116.
Le Ravalec, M., Guéguen, Y., 1996. High-and low-frequency elastic moduli for a saturated porous/cracked rock-differential self-consistent and poroelastic theories. Geophysics 61 (4), 1080–1094.
Lemaitre, J., 1984. How to use damage mechanics. Nucl. Eng. Des. 80 (2), 233–245.
Lemaitre, J., 1990. Mechanics of Solid Materials. Cambridge University Press, New York.
Li, H., Wang, Y., Liu, Z., 2004. Identification and determination of micro-crack size for frozen soil. Rock Soil Mech. 4 (25), 534–537.
Li, X., 2014. Rock Dynamics Fundamentals and Applications. Science Press, Beijing.
Li, X., Wang, S., Weng, L., Huang, L., Zhou, T., Zhou, J., 2015. Damage constitutive model of different age concretes under impact load. J. Cent. South Univ. 22 (2), 693–700.
Ma, D., Ma, Q., Yao, Z., Huang, K., 2019a. Static-dynamic coupling mechanical properties and constitutive model of artificial frozen silty clay under triaxial compression. Cold Reg. Sci. Technol. 167, 102858.
Ma, D., Ma, Q., Yao, Z., Yuan, P., Zhang, R., 2019b. Dynamic mechanical properties and failure mode of artificial frozen silty clay subject to one-dimensional coupled static and dynamic loads. Adv. Civ. Eng. 2019, 1–9.
Ma, D., Ma, Q., Yuan, P., 2017. SHPB tests and dynamic constitutive model of artificial frozen sandy clay under confining pressure and temperature state. Cold Reg. Sci. Technol. 136, 37–43.
Ma, W., Wang, D., 2012. Studies on frozen soil mechanics in china in past 50 years and their prospect. Chin. J. Geotech Eng. 34 (4), 625–640.
Mavko, G., Mukerji, T., Dvorkin, J., 2009. The Rock Physics Handbook. Cambridge University Press, New York.
Miao, T., Wei, X., Zhang, C., 1995. Creep of frozen soil by damage mechanics. Sci China B 38 (8), 996–1002.
Nemat-Nasser, S., Horii, H., 1982. Compression-induced nonplanar crack extension with application to splitting, exfoliation, and rockburst. J. Geophys. Res. 87 (B8), 6805–6821.
Qi, J., Ma, W., 2010. State-of-art of research on mechanical properties of frozen soils. Rock Soil Mech 31 (1), 133–143.
Rossi, P., Toutlemonde, F., 1996. Effect of loading rate on the tensile behaviour of concrete: description of the physical mechanisms. Mater. Struct. 29 (2), 116–118.

Schubnel, A., Guéguen, Y., 2003. Dispersion and anisotropy of elastic waves in cracked rocks. J. Geophys. Res. 108 (B2).
Taylor, L.M., Chen, E., Kuszmaul, J.S., 1985. Microcrack-induced damage accumulation in brittle rock under dynamic loading. Comput. Method. Appl. M. 55 (3), 301–320.
Wang, L., 2003. Stress wave propagation for nonlinear viscoelastic polymeric materials at high strain rates. Chin J. Mech. Ser. A. 19 (1), 177–183.
Wang, L., 2005. Foundation of Stress Waves. National Defense Industry Press, Beijing.
Wen, Z., Ma, W., Feng, W., Deng, Y., Wang, D., Fan, Z., Zhou, C., 2012. Experimental study on unfrozen water content and soil matric potential of qinghai-tibetan silty clay. Environ. Earth Sci. 66 (5), 1467–1476.
Xie, Q., Zhu, Z., Kang, G., 2016. A dynamic micromechanical constitutive model for frozen soil under impact loading. Acta Mech. Solida Sin. 29 (1), 13–20.
Yin, T., Wang, P., Yang, J., Li, X., 2018. Mechanical behaviors and damage constitutive model of thermally treated sandstone under impact loading. IEEE Access 6, 72047–72062.
Zhang, H., Liu, Y., Sun, H., Wu, S., 2016. Transient dynamic behavior of polypropylene fiber reinforced mortar under compressive impact loading. Constr. Build. Mater. 111, 30–42.
Zhang, H., Zhu, Z., Song, S., Kang, G., Ning, J., 2013. Dynamic behavior of frozen soil under uniaxial strain and stress conditions. Appl. Math. Mech. Engl. Ed. 34 (2), 229–238.
Zhang, M., Zhang, X., Lu, J., Pei, W., Wang, C., 2018. Analysis of volumetric unfrozen water contents in freezing soils. Exp. Heat Transfer. 32 (5), 1–13.
Zhang, Q., Zhao, J., 2014. A review of dynamic experimental techniques and mechanical behaviour of rock materials. Rock Mech. Rock Eng. 47 (4), 1411–1478.
Zhou, Z., Cai, X., Ma, D., Du, X., Chen, L., Wang, H., Zang, H., 2019. Water saturation effects on dynamic fracture behavior of sandstone. Int. J. Rock Mech. Min. 114, 46–61.
Zhu, Y., Zhang, J., Peng, W., Shen, Z., Miao, L., 1992. Constitutive relations of frozen soil in uniaxial compression. J. Glaciol. Geocryol. 14 (3), 210–217.
Zhu, Z., Liu, Z., Xie, Q., Lu, Y., Li, D., 2017. Dynamic mechanical experiments and microstructure constitutive model of frozen soil with different particle sizes. Int. J. Damage Mech. 27 (5), 686–706.
Zhu, Z., Ning, J., Ma, W., 2010. A constitutive model of frozen soil with damage and numerical simulation for the coupled problem. Sci. China-Phys. Mech. Astron. 53 (4), 699–711.